Journal of Innovative Optical Health Sciences
Vol. 7, No. 1 (2014) 1350028 (9 pages)

DOI: 10.1142/S1793545813500284

World Scientific
www.worldscientific.com

CHARACTERISTIC FEATURES OF MUELLER MATRIX PATTERNS FOR POLARIZATION SCATTERING MODEL OF BIOLOGICAL TISSUES

E DU[*,†], HONGHUI HE[*], NAN ZENG[*], CELONG LIU[*,†], YIHONG GUO[*,†], RAN LIAO[*], MINGHAO SUN[*,†], YONGHONG HE[*] and HUI MA[*,†,‡]

[*]*Shenzhen Key Laboratory for Minimal Invasive Medical Technologies, Graduate School at Shenzhen Tsinghua University, Shenzhen 518055, P. R. China*

[†]*Department of Physics, Tsinghua University, Beijing 100084, P. R. China*

[‡]*mahui@tsinghua.edu.cn*

Received 30 May 2013
Accepted 30 June 2013
Published 25 July 2013

We developed a model to describe polarized photon scattering in biological tissues. In this model, tissues are simplified to a mixture of scatterers and surrounding medium. There are two types of scatterers in the model: solid spheres and infinitely long solid cylinders. Variables related to the scatterers include: the densities and sizes of the spheres and cylinders, the orientation and angular distribution of cylinders. Variables related to the surrounding medium include: the refractive index, absorption coefficient and birefringence. In this paper, as a development we introduce an optical activity effect to the model. By comparing experiments and Monte Carlo simulations, we analyze the backscattering Mueller matrix patterns of several tissue-like media, and summarize the different effects coming from anisotropic scattering and optical properties. In addition, we propose a possible method to extract the optical activity values for tissues. Both the experimental and simulated results show that, by analyzing the Mueller matrix patterns, the microstructure and optical properties of the medium can be obtained. The characteristic features of Mueller matrix patterns are potentially powerful tools for studying the contrast mechanisms of polarization imaging for medical diagnosis.

Keywords: Mueller matrix; scattering; polarization; tissue; anisotropy.

1. Introduction

Recently, there have been growing interests in the applications of polarization imaging techniques for biomedical purposes. Mueller matrix provides a comprehensive representation for describing the polarization-related properties of the scattering media such as biological tissues. In the past decade, several groups have demonstrated that the Mueller

matrix imaging techniques have good potential in cancer detection.[1−5] However, the relations between Mueller matrix elements and structural properties of biological tissues are often not so clear, hindering further clinical applications of Mueller matrix polarimetric techniques to medical diagnosis. To interpret the relations adequately, we have to learn in detail the behaviors of polarized photons propagation in tissues. Monte Carlo simulations have been used as a powerful tool for analyzing the interactions between light and tissues. A proper optical scattering model is essential for such studies. A sphere only scattering model was used first for isotropic tissues such as blood, liver and fat.[6,7] Several groups studied the two-dimensional (2D) backscattering Mueller matrix patterns of such model.[8−10] Then the optical activity[11] and linear birefringence[12−14] for the ambient media were taken into account in the sphere optical activity model and sphere birefringence model. Using these models and Monte Carlo simulations, optical anisotropy properties (optical activity, linear birefringence, dichroism) of biological objects can be generated and studied. For instance, Angelsky *et al.* discussed the anisotropic complex biological tissue models and related possible diagnostic criteria.[15−19] To mimic the fibrous structures in biological tissues such as collagen fibers, muscle fibers and elastins, we proposed a sphere-cylinder scattering model (SCSM)[20,21] and studied the characteristic features of its backscattering Mueller matrix patterns.[22,23] Recently, SCSM has been expended to the comprehensive sphere-cylinder birefringence model (SCBM) to take into account of birefringent ambient medium.[24] A good agreement between the experimental and Monte Carlo simulated results has shown that the SCBM is a potentially powerful tool for biomedical imaging and diagnostic studies.

In this paper, we will summarize the developments of scattering models for biological tissues and introduce optical activity into the existing model. Using the model and Monte Carlo simulations we study the characteristic features of tissue-like media in detail. By comparing experiments and Monte Carlo simulations, we analyze the backscattering Mueller matrix patterns of several tissue-like media, and summarize the different effects coming from anisotropic scattering and optical properties (optical activity, linear birefringence). In addition, we study the possible method to extract the optical activity values for tissues. Both the experimental and simulated results show that, by analyzing the Mueller matrix patterns, the microstructures and optical properties of the medium can be obtained. The characteristic features of Mueller matrix patterns are potentially powerful tools for studying the mechanisms of polarization imaging for biomedical diagnosis.

2. Methods: Monte Carlo Simulation and Experiments

2.1. *Scattering model for biological tissues*

As shown in Fig. 1, the scattering model for biological tissues is a homogeneous medium consisting of microspheres and infinitely long cylindrical scatterers. Parameters of the scatterers, such as their sizes, refractive indices and densities can be varied independently. The orientations of the cylinders are also variable. It is assumed that the orientation angle of the cylinders follows a Gaussian distribution. In addition, parameters of the surrounding media, such as refractive index, absorption coefficient, optical rotation degree (ORD), birefringence value and birefringence axis, are all variables in the model.

2.2. *Monte Carlo simulation*

In our previous works, a Monte Carlo program has been developed to track down scattering and propagation behavior of each polarized photon.[20,24] In Monte Carlo simulations for SCBM, the program starts by launching a normal incident photon at an initial position and direction. The polarization state of this photon is represented by a Stokes vector. The

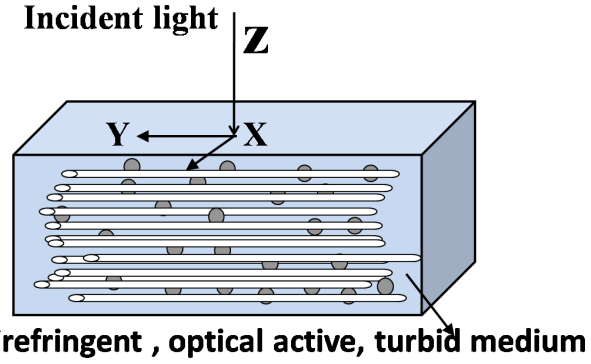

Fig. 1. Schematics of the scattering model for biological tissues.

photon propagates in a linearly birefringent medium until it is scattered or absorbed. The polarization state and position of the photon are both updated. At each scattering point, the photon drops part of its energy due to the absorption. A statistical method has been designed to determine whether the photon is scattered by the cylinders or the spherical particles. Then the scattering direction is calculated depending on the phase function with a random number. The simulation process will continue until a photon is completely absorbed or move out of the sample. All the information of the emitted photons will be stored, including their polarization states, positions and emitted directions.

In this paper, as a development to SCBM, we add a new module to the model and Monte Carlo program to calculate the effects of optical activity. Optical activity does not affect the scattering process, but it alters the polarization states of photons as their propagation between two successive scattering events.[11,14] The new module calculates the changes of Stokes vector due to the optical activity medium as Eq. (1):

$$S' = R(\theta) \cdot S. \tag{1}$$

In Eq. (1), $R(\theta)$ represents the rotational matrix, which can be expressed as Eq. (2):

$$R(\theta) = \begin{bmatrix} 1 & 0 & 0 & 0 \\ 0 & \cos 2\theta & -\sin 2\theta & 0 \\ 0 & \sin 2\theta & \cos 2\theta & 0 \\ 0 & 0 & 0 & 1 \end{bmatrix}. \tag{2}$$

In Eq. (2), θ represents the rotational angle which can be obtained as Eq. (3):

$$\theta = \chi \cdot s = \mathrm{ORD} \cdot \alpha \cdot s. \tag{3}$$

In Eq. (3), χ is the product of the ORD and the concentration of optical active molecules (α). ORD represents the rotatory power of the optical active molecules. S is the path length of light.

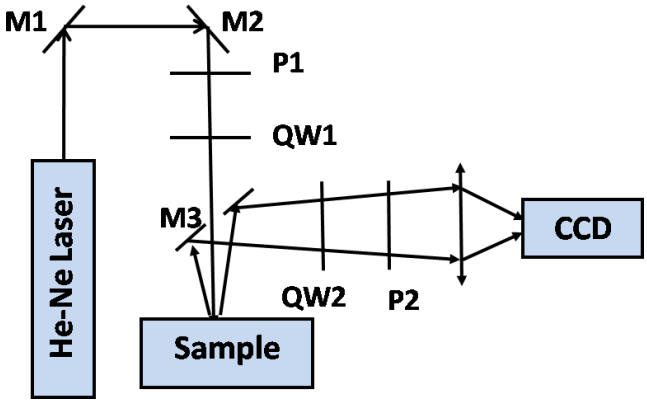

Fig. 2. A schematic of the experimental setup. P, polarizer; QW, quarter-wave plate; CCD, imaging camera.

2.3. *Experimental setup*

The typical backscattering Mueller matrix measurement experimental setup used in this paper is shown in Fig. 2.[9] The light source is a 633 nm linearly polarized He−Ne laser (Daheng Optics, China, DH-HN600). A set of quarter-wave plate (QW1) (Daheng Optics, China, GCL-060402) and linear polarizer P1 (Daheng Optics, China, GCL-050003, extinction ratio 500:1) is used to change the polarization states of incident light. The polarization states of scattered light can be measured by a second set of quarter-wave plate (QW2) and linear polarizer (P2). The backscattering photons are recorded by an 8 bit CCD camera (Canon EOS 550D) to produce reflectance images of the samples. In this paper, for the measurements of Mueller matrix, six different polarization states are achieved for the incident light: 0° linear (H), 90° linear (V), 45° linear (P), 135° linear (M), right circular (R) and left circular (L), then six polarization components of scattered light corresponding to each incident state are recorded. A total of 36 reflectance images are captured and the Mueller matrix can be calculated from the reflectance images as Eq. (4). The Mueller matrix elements are all normalized by the maximum intensity of the $m11$.

$$M = \begin{pmatrix} m11 & m12 & m13 & m14 \\ m21 & m22 & m23 & m24 \\ m31 & m32 & m33 & m34 \\ m41 & m42 & m43 & m44 \end{pmatrix}$$
$$= \frac{1}{2} \begin{pmatrix} HH + HV + VH + VV & HH + HV - VH - VV & PH + PV - MP - MM & RH + RV - LH - LV \\ HH - HV + VH - VV & HH - HV - VH + VV & PH - PV - MH + MV & RH - RV - LH + LV \\ HP - HM + VP - VM & HP - HM - VP + VM & PP - PM - MP + MM & RP - RM - LP + LM \\ HR - LL + VR - RL & HR - VR + VL - HL & PR - MR + ML - PL & RR - RL - LR + LL \end{pmatrix}. \tag{4}$$

In Eq. (4), the first letter represents the input polarization state and the second letter represents the output polarization state. For example, "HV" represents a vertically-polarized (V) reflectance image with horizontally-polarized (H) incident light.

3. Results and Discussion

As introduced above, the polarization scattering model for biological tissues includes both spherical and infinitely long cylindrical scatterers, the optical activity and birefringence effects. According to characteristics of different biological tissues, the model can be adjusted. Based on this model, using both the experiments and Monte Carlo simulations, we studied the 2D backscattering Mueller matrix patterns for different types of scattering media, which include: the sphere scattering medium, the sphere birefringence medium, the sphere-cylinder scattering medium, the sphere-cylinder birefringence medium and the sphere optical activity medium. We analyzed the characteristic features of 2D Mueller matrix elements patterns, and summarized the different effects coming from anisotropic scattering and optical properties.

3.1. *Comparison of cylindrical scattering and birefringence effects*

The experimental and Monte Carlo simulated results of different media are shown in Figs. 3 and 4. It can be observed that the simulated results agree well with the experimental measurements, showing the validity of the scattering model and Monte Carlo simulations. Figures 3(a) and 4(a) show the experimental and simulated 2D Mueller matrix patterns for the sphere scattering medium, which consists of $0.2\,\mu$m diameter polystyrene microspheres (International Laboratory, USA, $\mu_s = 10\,\text{cm}^{-1}$, $n = 1.59$) suspending in water. Figures 3(b) and 4(b) show the experimental and simulated 2D Mueller matrix patterns for the sphere birefringence medium, which

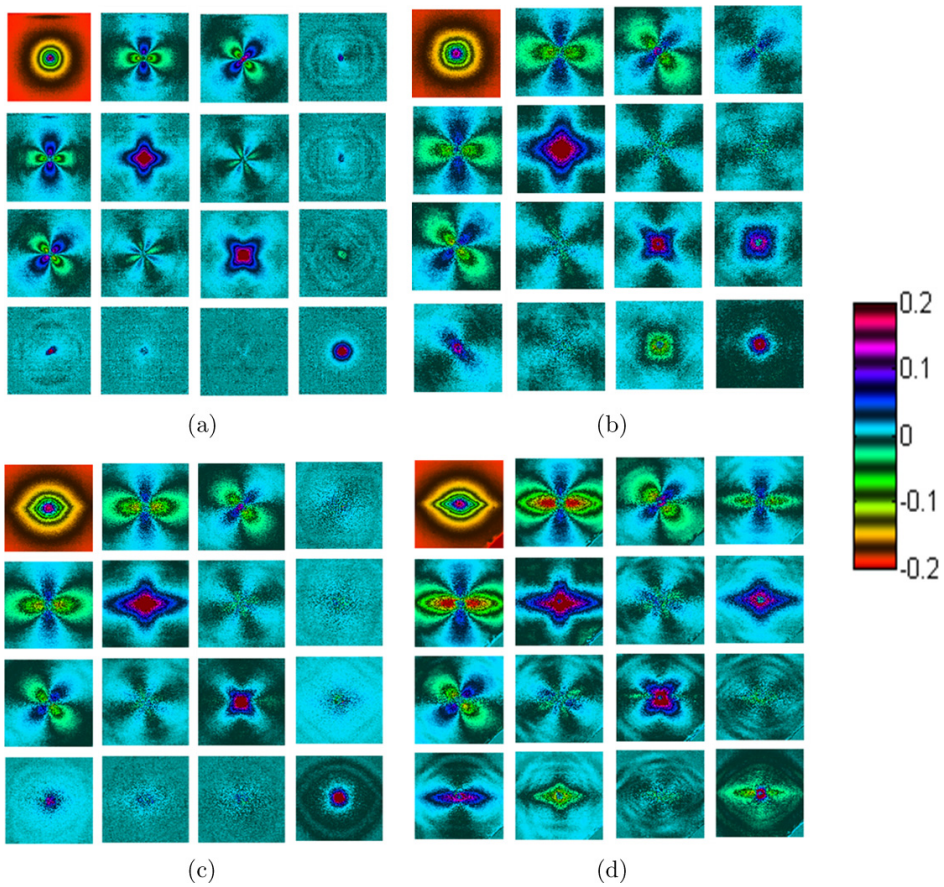

Fig. 3. Experimental backscattering Mueller matrices of (a) sphere scattering medium, (b) sphere birefringence medium, (c) sphere-cylinder scattering medium and (d) sphere-cylinder birefringence medium.

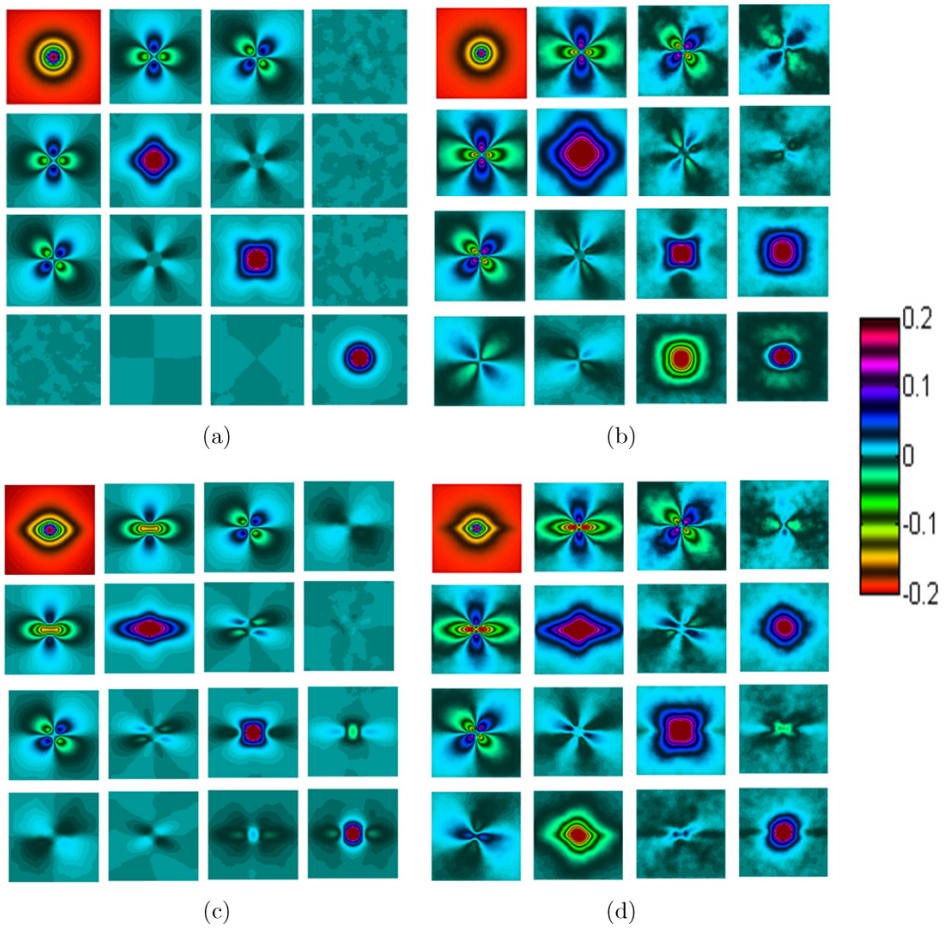

Fig. 4. Monte Carlo simulated backscattering Mueller matrices of (a) sphere scattering medium, (b) sphere birefringence medium, (c) sphere-cylinder scattering medium and (d) sphere-cylinder birefringence medium.

is an extended hydrogel cuboid with 0.2 μm diameter polystyrene microspheres ($\mu_s = 5\,\text{cm}^{-1}$, $n = 1.59$) immersed in it.[14] The extraordinary axis of the birefringent sample (the extended direction of the hydrogel) is along the x-axis. The birefringence value of the elongated hydrogel sample is 1×10^{-5} responding to the extension of 5 mm. Figures 3(c) and 4(c) show the experimental and simulated 2D Mueller matrix patterns for the sphere-cylinder scattering media. The sample used in experiments is a three-layered medium consisting of both well-aligned silk fibers along the y-axis and microspheres submerged in water. The first and third layers are 5 mm thick solutions of 0.2 μm diameter polystyrene microspheres ($\mu_s = 5\,\text{cm}^{-1}$, $n = 1.59$). The second layer contains only well-aligned silk fibers (provided by Guangxi Institute of Supervision and Testing on Product Quality) along the y-axis. The thickness of the silk fibers is 1 mm. The diameters, scattering coefficient and refractive index of the silk fibers are 1.5 μm, 65 cm^{-1} and 1.56, respectively.[22] Figures 3(d) and 4(d) show the experimental and simulated 2D Mueller matrix patterns for the sphere-cylinder birefringence media. The experimental sample is the three-layered microsphere-silk medium submerged in an extended hydrogel. The birefringence value of this sample is 1×10^{-5} responding to the extension of 5 mm. The birefringence axis (the direction of strain) is along 45° direction on the X-Y plane.[24]

The experimental and simulated results shown in Figs. 3 and 4 demonstrate that the cylindrical scattering and birefringence effects affect Mueller matrix elements differently. The $m11$ element relates only to unpolarized light intensity, which is not affected by the linear birefringence. Therefore, comparing with the sphere scattering medium [see Figs. 3(a) and 4(a)], the $m11$ element for the sphere birefringence medium [see Figs. 3(b) and 4(b)] has the same circular characteristics. Since the $m12$,

$m21$ and $m22$ elements relate to horizontal and vertical polarization components, when the birefringence axis is along x or y direction, these elements are also not affected. However, compared to the sphere scattering medium, other Mueller matrix elements are affected by birefringence. The birefringence effects destroy the rotational symmetry of the $m12/m13$, $m21/m31$ and $m22/m33$ pairs which exists in the sphere scattering medium. The total intensity values of the $m12$, $m21$ and $m22$ elements become larger than those of the $m13$, $m31$ and $m33$ elements. The $m14$ ($m41$), $m24$ ($m42$) and $m34$ ($m43$) elements have similar shapes as those of the $m13$, $m23$ and $m33$ elements, respectively. This is because the transformation between circular polarization state and 45° linear polarization state in the medium is enhanced by the linear birefringence.[12] The $m14$ and $m41$ elements always keep the quatrefoil patterns, but rotate as the birefringence axis changes. Moreover, as the birefringence value varies, the absolute intensity of the $m14$ and $m41$ elements also changes. In short, the $m14$ and $m41$ elements can be used to determine the value and direction of birefringence.[13]

Different from the birefringence effects discussed above, the cylindrical scattering affects all the Mueller matrix elements. Comparing with the sphere scattering medium [see Figs. 3(a) and 4(a)], for the sphere-cylinder scattering medium [see Figs. 3(c) and 4(c)], the intensity distributions of the $m11$, $m12$, $m21$ and $m22$ elements along the x-axis become larger than those along the y-axis due to the cylindrical scattering effect.[21,22] For instance, the cylinders result in more photons being scattered to the x-axis direction, leading to a rhombic $m11$ shape in Figs. 3(c) and 4(c). Patterns of the $m11$ element can be used to judge the presence of the cylindrical scatterers.[21–24] Besides, the cylindrical scattering effect also destroys the rotational symmetry of the $m12/m13$, $m21/m31$ and $m22/m33$ pairs. The total intensity values of the $m12$, $m21$ and $m22$ elements become larger than those of the $m13$, $m31$ and $m33$. These changes are similar as those coming from the birefringence effect.

For the sphere-cylinder birefringence medium, both the cylindrical scattering and birefringence affect the Mueller matrix elements simultaneously. As shown in Figs. 3(d) and 4(d), the $m11$ element has rhombic shape due to the cylindrical scattering. The $m14$ and $m41$ elements keep the quatrefoil patterns and rotate by 45° with the birefringence axis. The Mueller matrix elements can be used to reveal the structural and optical properties of the media containing cylinders and birefringence.

3.2. *Mueller matrix patterns of optical active medium*

Besides spherical, cylindrical scatterers and birefringence effect, some tissues contain chiral molecules such as glucose. Therefore, the patterns of Mueller matrix for a sphere optical active medium should be studied. Figure 5(a) shows the experimental backscattering Mueller matrix of a sample

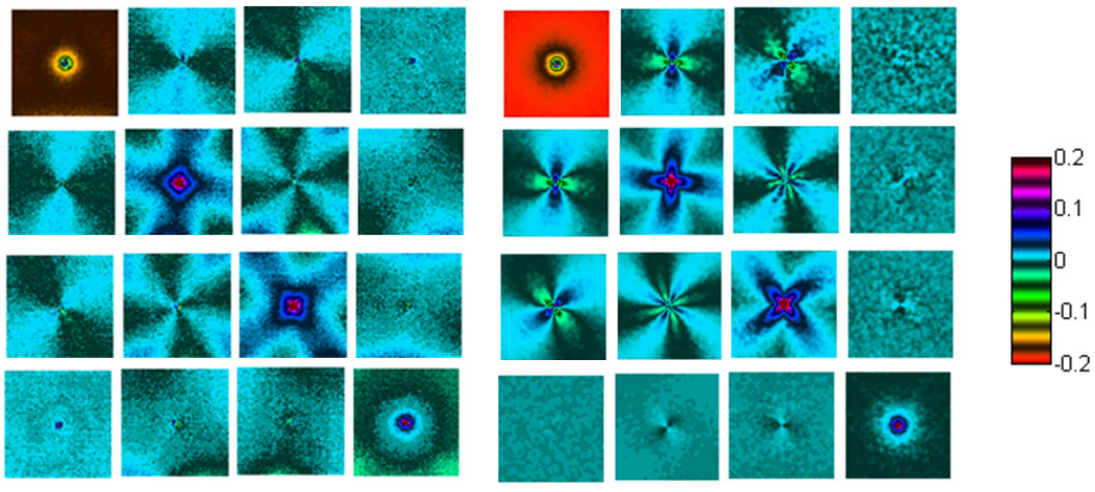

(a) (b)

Fig. 5. Backscattering Mueller matrices for sphere optical active medium: (a) experimental result of microsphere sucrose solution and (b) Monte Carlo simulated results.

containing 2 μm diameter polystyrene microspheres ($\mu_s = 5\,\mathrm{cm}^{-1}$, $n = 1.59$) in sucrose solution ($\chi = 5.37\,\mathrm{deg\ cm}^{-1}$, $n = 1.45$), Fig. 5(b) shows the corresponding Monte Carlo simulated results. The good agreement between experimental and simulated results shows the validity of the optical active module for the Monte Carlo program.

Similar as the sphere scattering medium [see Figs. 3(a) and 4(a)], for the sphere optical active medium the patterns of the $m11$ and $m44$ elements are groups of circles, the $m14$ and $m41$ elements are blanks. It can be observed that the optical activity does not affect the $m11$, $m14$, $m41$ and $m44$ elements, which only relate to unpolarized light and circular polarized light. The chiral sucrose molecules prominently change the polarization states of the linear polarized light. Hence, the optical activity affects the other Mueller matrix elements relating to the linear polarization states. The patterns of these elements have obvious different rotations around the incident point, which is at the center of each map. The diagonal symmetry properties of the Mueller matrix elements are destroyed because of the existence of chiral molecules. However, the optical activity effect does not destroy the rotational symmetry of the $m12/m13$, $m21/m31$ and $m22/m33$ elements pairs. While, the symmetry of the $m12/m21$, $m13/m31$, $m24/m42$ and $m34/m43$ elements pairs are damaged. The rotation angle of the $m21/m31/m24/m34$ becomes larger than that of the $m12/m13/m42/m43$ at the same detection position.[11] Among all the 16 Mueller matrix elements, the rotation effects of the $m22$, $m23$, $m32$ and $m33$ elements are the most obvious. Therefore, patterns of the $m22/m33/m23/m32$ elements can be used to detect the existence of the optical activity in a medium.

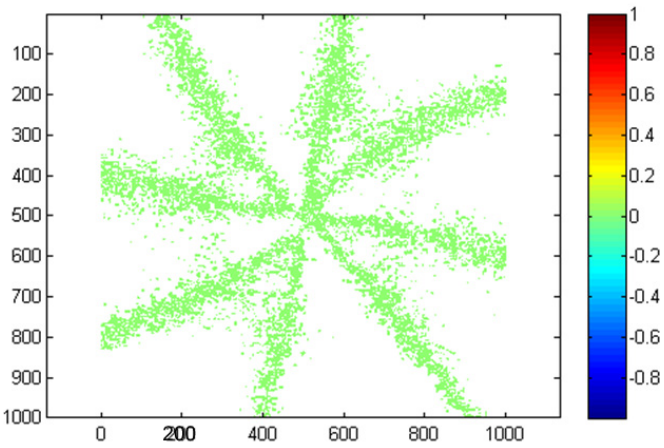

(a)

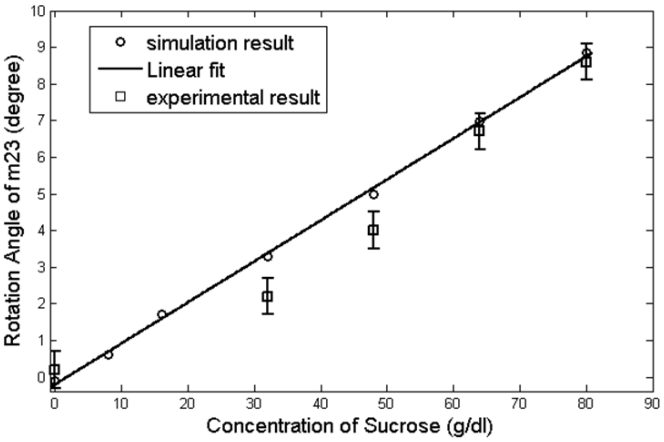

(b)

Fig. 6. Backscattering Mueller matrix element $m23$ for sphere optical active medium: (a) zero-intensity profile of the $m23$ and (b) rotation angle of the $m23$ change with the concentration of sucrose.

3.3. *Effect of optical active molecules' concentration on Mueller matrix patterns*

Furthermore, we analyze the effect of the optical active molecules' concentration on the 2D Mueller matrix patterns quantitatively. As mentioned in Sec. 3.2, the most sensitive Mueller matrix elements are the $m22$, $m23$, $m33$ and $m32$. In this section, we choose the $m23$ as the analyzing example. Figure 6(a) shows the zero-intensity profiles of the $m23$ element. It can be observed that the equi-intensity profiles of the $m23$ are approximately straight lines. We fit these lines using least square method and compare them with those of the sphere scattering medium. Then we can obtain the rotation angle of the $m23$ due to optical activity.

For the study of relationship between the rotation angle of the $m23$ and the value of optical activity, we change the concentration of sucrose in both the experiments and Monte Carlo simulations. The experimental and simulated results are shown in Fig. 6(b). It can be seen that as the concentration of sucrose increases, the rotation angle of the $m23$ also increases. Although there is discrepancy between the experimental and the simulated results because of the limited accuracy of measurements,

the results show that the rotation angle of the $m23$ correlates to the sucrose's concentration linearly. Therefore, the $m23/m32$ can be used to determine the concentration of the optical active molecules quantitatively. However, it should be pointed out that such measurement works only for very high concentration. When the concentration of sucrose is less than 32 g/dl, the rotation of the $m23$ can hardly be observed.

4. Conclusions

We have developed a model to describe polarized photons scattering in biological tissues. In this model, tissues are simplified to a mixture of scatterers and surrounding medium. There are two types of scatterers: solid spheres and infinitely long solid cylinders. The densities and sizes of the spheres and cylinders, the orientation, angular distribution of the cylinders are variable. The refractive index, absorption coefficient and birefringence of the surrounding medium can also be varied. In this paper, we introduced optical activity into the existing module and summarized the characteristic features in the 2D backscattering Mueller matrix patterns due to different constituents in the model. By comparing experiments and Monte Carlo simulations, we analyzed the backscattering Mueller matrix patterns of several tissue-like media, which include the sphere scattering medium, the sphere birefringence medium, the sphere-cylinder scattering medium, the sphere-cylinder birefringence medium and the sphere optical active medium. Moreover, we summarized the different effects coming from anisotropic scattering and optical properties, and proposed a possible method to extract the optical activity values for tissues. For example, the $m11$ element can be used as an indicator for the concentration of cylindrical scatterers. The $m14/41$ and $m22/m33/m23/m32$ elements can be used to indicate the existence of the birefringence and the optical activity effects, respectively. In summary, this polarization scattering model is a potentially powerful tool in studying the contrast mechanisms of polarization imaging techniques for biomedical purposes.

Acknowledgments

This work has been supported by National Natural Science Foundation of China (NSFC) Grants No. 10974114, 11174178, 41106034, and Open Fund of Key Laboratory of Optoelectronic Information and Sensing Technologies of Guangdong Higher Education Institutes, Jinan University.

References

1. P. Shukla, A. Pradhan, "Mueller decomposition images for cervical tissue: Potential for discriminating normal and dysplastic states," *Opt. Express* **17**(3), 1600−1609 (2009).
2. M. Antonelli, A. Pierangelo, T. Novikova, P. Validire, A. Benali, B. Gayet, A. Martino, "Mueller matrix imaging of human colon tissue for cancer diagnostics: How Monte Carlo modeling can help in the interpretation of experimental data," *Opt. Express* **18**(10), 10200−10208 (2010).
3. A. Pierangelo, A. Benali, M. Antonelli, T. Novikova, P. Validire, B. Gayet, A. Martino, "Ex-vivo characterization of human colon cancer by Mueller polarimetric imaging," *Opt. Express* **19**(2), 1582−1593 (2011).
4. A. Pierangelo, S. Manhas, A. Benali, C. Fallet, J. Totobenazara, M. Antonelli, T. Novikova, B. Gayet, A. Martino, P. Validire, "Multispectral Mueller polarimetric imaging detecting residual cancer and cancer regression after neoadjuvant treatment for colorectal carcinomas," *J. Biomed. Opt.* **18**(4), 046014 (2013).
5. H. He, N. Zeng, D. Li, R. Liao, H. Ma, "Quantitative Mueller matrix polarimetry techniques for biological tissues," *J. Innov. Opt. Health Sci.* **5**(3), 1250017 (2012).
6. M. Yamanari, Y. Yasuno, T. Yatagai, M. Itoh, "Analysis of the polarization dependence of multiple backscattering light from red blood cells," *Proc. SPIE* **5695**, 58−65 (2005).
7. V. Sankaran, K. Schönenberger, J. T. Walsh, Jr., D. J. Maitland, "Polarization discrimination of coherently propagating light in turbid media," *Appl. Optics.* **38**(19), 4252−4261 (1999).
8. B. D. Cameron, M. J. Rakovic, M. Mehrübeoglu, G. W. Kattawar, S. Rastegar, L. V. Wang, G. L. Coté, "Measurement and calculation of the two-dimensional backscattering Mueller matrix of a turbid medium," *Opt. Lett.* **23**(7), 485−487 (1998).
9. M. J. Rakovic, G. W. Kattawar, M. Mehrubeoglu, B. D. Cameron, S. Rastegar, L. V. Wang, G. L. Coté, "Light backscattering polarization patterns from turbid media: Theory and experiment," *Appl. Opt.* **38**(15), 3399−3408 (1999).
10. Y. Deng, S. Zeng, Q. Luo, Z. Zhang, L. Fu, "Numerical study of the effects of scatterer sizes and distributions on multiple backscattered intensity

patterns of polarized light," *Opt. Lett.* **33**(1), 77−79 (2008).
11. X. Wang, G. Yao, L. V. Wang, "Monte Carlo model and single-scattering approximation of the propagation of polarized light in turbid media containing glucose," *Appl. Opt.* **41**(4), 792−801 (2002).
12. X. Wang, L. V. Wang, "Propagation of polarized light in birefringent turbid media: A Monte Carlo study," *J. Biomed. Opt.* **7**(3), 279−290 (2002).
13. C. Baravian, J. Dillet, F. Caton, J. P. Decruppe, "Birefringence determination in turbid media," *Phys. Rev. E* **75**(3), 032501 (2007).
14. M. F. G. Wood, X. Guo, I. A. Vitkin, "Polarized light propagation in multiply scattering media exhibiting both linear birefringence and optical activity: Monte Carlo model and experimental methodology," *J. Biomed. Opt.* **12**(1), 014029 (2007).
15. O. V. Angelsky, A. G. Ushenko, Y. G. Ushenko, Y. Y. Tomka, "Polarization singularities of biological tissues images," *J. Biomed. Opt.* **11**(5), 054030 (2006).
16. O. V. Angelsky, Y. Y. Tomka, A. G. Ushenko, Y. G. Ushenko, Y. A. Ushenko, "Investigation of 2D Mueller matrix structure of biological tissues for preclinical diagnostics of their pathological states," *J. Phys. D-Appl. Phys.* **38**(23), 4227−4235 (2005).
17. O. V. Angelsky, G. V. Demianovsky, A. G. Ushenko, D. N. Burkovets, Y. A. Ushenko, "Wavelet analysis of two-dimensional birefringence images of architectonics in biotissues for diagnosing pathological changes," *J. Biomed. Opt.* **9**(4), 679−690 (2004).
18. Y. A. Ushenko, O. I. Telenga, A. P. Peresunko, O. K. Numan, "New parameter for describing and analyzing the optical-anisotropic properties of biological tissues," *J. Innov. Opt. Health Sci.* **4**(4), 463−475 (2011).
19. O. V. Angelsky, A. G. Ushenko, Y. A. Ushenko, "Investigation of the correlation structure of biological tissue polarization images during the diagnostics of their oncological changes," *Phys. Med. Biol.* **50**(20), 4811−4822 (2005).
20. T. Yun, N. Zeng, W. Li, D. Li, X. Jiang, H. Ma, "Monte Carlo simulation of polarized photon scattering in anisotropic media," *Opt. Express* **17**(19), 16590−16602 (2009).
21. H. He, N. Zeng, R. Liao, T. Yun, W. Li, Y. He, H. Ma, "Application of sphere−cylinder scattering model to skeletal muscle," *Opt. Express* **18**(14), 15104−15112 (2010).
22. H. He, N. Zeng, W. Li, T. Yun, R. Liao, Y. He, H. Ma, "Two dimensional backscattering Mueller matrix of sphere−cylinder scattering medium," *Opt. Lett.* **35**(14), 2323−2325 (2010).
23. H. He, N. Zeng, E. Du, Y. Guo, D. Li, R. Liao, Y. He, H. Ma, "Two-dimensional and surface backscattering Mueller matrices of anisotropic sphere-cylinder scattering media: A quantitative study of influence from fibrous scatterers," *J. Biomed. Opt.* **18**(4), 046002 (2013).
24. E. Du, H. He, N. Zeng, Y. Guo, R. Liao, Y. He, H. Ma, "Two-dimensional backscattering Mueller matrix of sphere−cylinder birefringence media," *J. Biomed. Opt.* **17**(12), 126016 (2012).